HEFAT2007
5th International Conference on Heat Transfer, Fluid Mechanics and Thermodynamics
Sun City, South Africa
Paper number: HJ2

THERMAL CHARACTERISTICS OF HIGH-CURRENT VACUUM ARCS OF THE AXIAL MAGNETIC FIELD CONTACTS

J.–H. Hwang[1], J.–C. Lee[2], M.–J. Choi[3], J.–R. Kwon[3] and Y.–J. Kim[4]*
[1]Graduate School of Mechanical Engineering, Sungkyunkwan University
[2]School of Mechanical & Automotive Engineering, Kangnung National University
[3]Electro-Mechanical Research Institute, Hyundai Heavy Industries Co., LTD.
[4]*(Author for correspondence)
School of Mechanical Engineering, Sungkyunkwan University,
300 Cheoncheon-dong, Suwon 440-746, KOREA
E-mail: yjkim@skku.edu

ABSTRACT

The capabilities and advantages of vacuum interrupters (VIs) have been widely recognized on switching and controlling the fault currents in medium voltage level. Due to its environmental friendliness, there were various research and developments for using VIs in transmission and distribution lines. An axial magnetic field (AMF) electrode has more advantages of the switching capability than other contact designs such as reducing the arc voltage, securing higher current value for transferring from the constriction arc to the diffused arc and regulating the arc current distribution. The arc constriction should increase the heat flux and the local temperature on the electrodes and result in the surface melting, which has undesirable influences on the characteristics of vacuum arc and surroundings. In the present study, we considered two different types of AMF electrodes used widely in industries, one is coil type and the other is cup type, to investigate the effective arc area and the thermal characteristics by high-current vacuum arcs through three-dimensional FEM analysis. Calculated results were compared with the results by a commercial package, MAXWELL 3D, which is a reliable analysis tool for the electro-magnetic fields, to validate the present calculation.

INTRODUCTION

Vacuum circuit breakers (VCBs) have been commercially attractive as a means to interrupt short-circuit currents in medium voltage networks. The interrupter, which consists of two electrodes, metal shield, bellows and ceramic insulator, is the most important part to accomplish the performance of VCBs. In case of the plain butt shape contacts, it was recognized to have a limited performance for interrupting high-currents due to the arc constriction. It is known that the arc happens to be constricted at the current of approximately 10kA and forms the anode spots which caused the electrode melting and some harmful effects to the interruption capacity. Therefore, it will be clear that the anode spots should be avoided as less as possible to raise the interruption current limit of VCBs. One way for avoiding the excessive electrode erosion is to produce a transverse magnetic field (TMF or RMF) across the electrodes and to move the arc column along the surface by Lorentz force. Another approach is to produce AMF across the contacts and to increase the current limitation value on the arc constriction [1].

In general, one typical feature of vacuum arcs in the high currents is columnar arc [2]. In a stationary columnar mode, the vacuum arc makes the gross erosion of electrodes that leads to considerable metal vapour density in the interelectrode gap. It is well known that vacuum arcs remain in a diffuse mode up to sufficiently high current when a uniform AMF in the gap is imposed. In that case, the arc current-voltage characteristics are dependent on the AMF intensity [3-6].

The overall plasma expansion progress is as following. After the rupture of the molten metal bridge, the confined arc forms, and this arc slowly expands into a diffused arc which burns until current zero. Once the arc has been diffused, a large enough AMF allows the arc to remain diffuse. The electrons are confined by the magnetic field lines in the intercontact region and, because of the associated creation of radial electric fields, the ions are also confined to the intercontact region. During this high-current arcing, the diffused arc distributes the arc energy over the whole contact surface and thus prevents the gross erosion of electrodes [7].

In order to consider the effect of contact geometries for AMF numerically, we used two different types of AMF electrodes to investigate the effective arc area (A_{eff}) and the thermal characteristics by high-current vacuum arcs through three-dimensional FEM analysis. The detail approach on the thermal characteristics of vacuum arcs is in progress with 3-D coupled field analysis for the practical prediction.

NOMENCLATURE

A	[-]	Magnetic vector potential
A_{eff}	[m^2]	Effective arc area
B	[T]	Magnetic flux density vector
D	[C/m^2]	Electric flux density vector
d	[m]	Diameter of the contact
E	[V/m]	Electric field intensity vector
H	[A/m]	Magnetic field intensity vector
I	[A]	Current
J	[A/m^2]	Current density vector
l	[m]	Interelectrode gap distance
t	[sec]	Time

Special characters

θ	[rad]	Phase angle ($\theta = \omega t$)
μ	[N/A^2]	Magnetic permeability ($\mu = B / H$)
μ_r	[-]	Relative permeability ($\mu_r = \mu / \mu_0$)
ν	[A^2/N]	Reluctivity
σ	[S/m]	Electric conductivity
Φ	[V]	Electric potential
ω	[rad/sec]	Angular velocity

Subscripts

0	Zero value of an AC current
crit	Critical value
o	Input current vector component
e	Eddy current vector component
p	Peak value of an AC current
rms	Root-mean-square
z	Cartesian axis direction

NUMERICAL ANALYSIS

The first commercial VI imposed on AMF electrode was developed by Toshiba Corporation [8]. Thereafter, various AMF electrodes, such as cup-type electrodes, tubular electrodes [9], horse-shoe shapes [10], and multipole electrodes [11-12], etc., have been designed to achieve the lower Joule loss, weaker residual AMF after current zero, and especially, higher interruption capacity with smaller dimension.

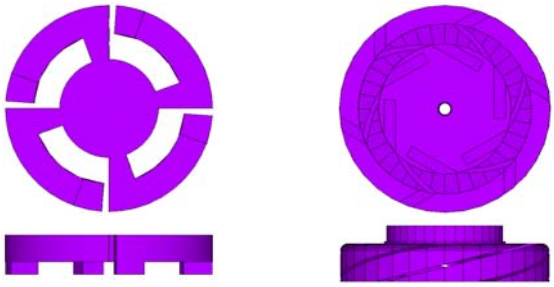

(a) electrode coil (left) and cup (right)

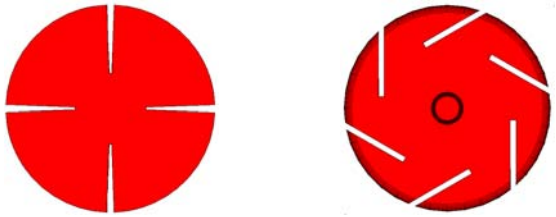

(b) contact plate

Figure 1 Configuration of the numerical models.
(left: Type 1 – coil type, right: Type 2 – cup type)

Table 1 Material properties of each components in the VI.

Components	Material	σ (S/m)	μ_r
1) Vacuum	Air	1.0E-9	1.0
2) Conductor and electrode	Cu	5.8E+7	
3) Contact plate	CuCr50	1.276E+7	
4) Arc column	Arc	1.0E+4	

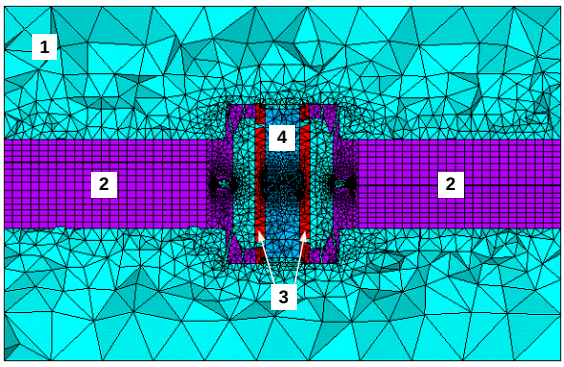

Figure 2 Grid systems of the modelled VI.

In order to take into account the effect of the contact shapes, we selected two kinds of AMF contacts based on segments coil-type (Type 1) and cup-type (Type 2) AMF contact, as shown in Fig. 1. The numerical simulations concern the diffused arc mode dominantly, and the simulations are conducted at the alternating current (AC, I=30kA_{rms}) and the fixed gap distance (l=20mm). In the case of Type 1, its configuration is based on the elsewhere [13], and we determined its detail dimensions which are identical to our own model (Type 2). The effective contact diameter is 84mm and both of two types have same material properties as listed in Table 1.

One example of grid systems (Type 2) is depicted in Fig. 2. The domain of all elements in the modelled VI is composed of hybrid grid systems in order to establish a discrete system for numerical simulation. There are total four different regions according to each material property as follows; 1) vacuum, 2) conductor and electrode, 3) contact plate and 4) arc column. Here, the arc column is modelled as a cylindrical shape with the same diameter of the electrode and with the constant electric conductivity. The total hybrid elements are nearly 175,000 for Type 1 and 310,000 for Type 2, respectively. Since Type 2 has more complicated cup-type coil part, it produces larger number of element than Type 1.

The electro-magnetic phenomena can be described by the three-dimensional, transient Maxwell's equations as follows:

$$\nabla \times H = J_o + J_e,\ J_e = \sigma E_e \tag{1}$$

$$\nabla \times (E_e + \partial A / \partial t) = 0 \tag{2}$$

Here, J_e is an eddy current density, E_e is an electron-induced electric field, respectively. Since Eq. (2) presents the case of conservative field, Eqs. (1) and (2) can be rewritten as follows:

$$E_e = -\partial A / \partial t - \nabla \phi \quad (3)$$

$$J_e = -\sigma(\partial A / \partial t) - \sigma \nabla \phi \quad (4)$$

Thus the governing equation of the transient magnetic vector potential which includes the eddy current can be defined as,

$$\nabla \times (\nu \nabla \times A) = J_o + J_e = J_o - \sigma(\partial A / \partial t) - \sigma \nabla \phi \quad (5)$$

Here, ν is the permittivity, σ is the electric conductivity and ϕ is the electric potential, respectively.

We calculated the transient magnetic fields in the VI with three-dimensional FEM code, ANSYS, taking into account eddy current effect. The computation condition is: the opening stroke is 20mm, and the excitation source of each model was 30kA$_{rms}$-60Hz AC circuit. The ground condition (ϕ=0V) was applied at the opposite side of the conduct rod. At all outside walls, the magnetic flux parallel condition (A_Z=0) was set to constrain all degree of freedoms (DOFs). The Jacobi Conjugate Gradient (JGC) solver was used, and its convergence criterion was set to 1.0e-9.

RESULTS AND DISCCUTION

It is the purpose of the magnetohydrodynamic (MHD) approaches to calculate the magnetic and thermal-flow fields by the coupled calculation, simultaneously. By the electro-magnetic analysis for an advance work of MHD solution, the magnetic field properties and Joule heat generations as the input parameters for the thermal-flow analysis can be obtained. Former given a system of Maxwell's equations are coupled and solved iteratively by a finite element method with a transient condition.

In order to validate the calculation method, two series of results on the cup-type AMF are compared: (A) indicates the calculation results by ANSYS E-MAG, and (M) by MAXWELL 3D which is widely used in the electro-magnetic

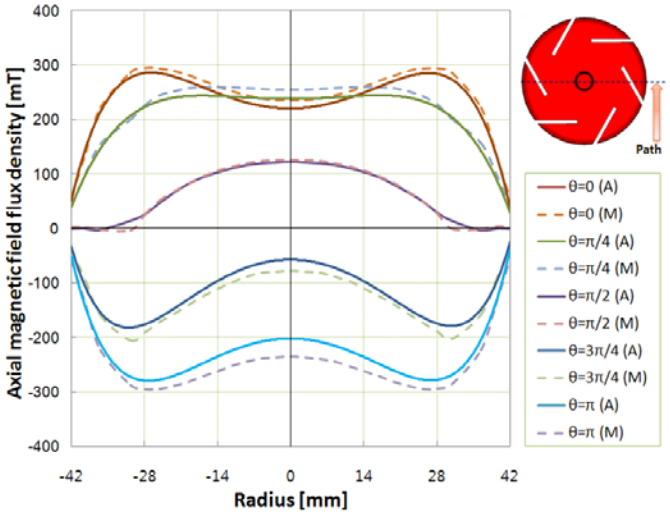

Figure 3 Comparison between two series of calculated results (A): ANSYS E-MAG, (M): MAXWELL 3D

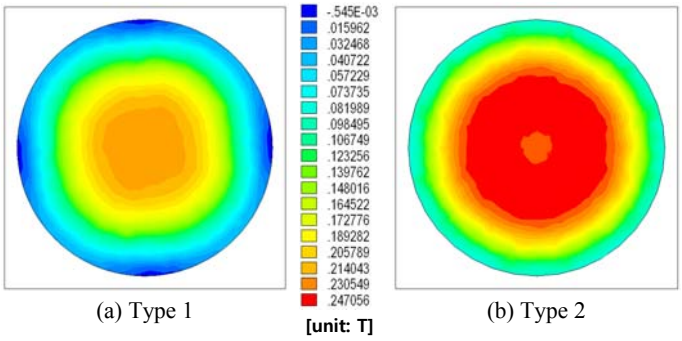

(a) Type 1 (b) Type 2

Figure 4 AMF distributions on the intermediate plane of the gap at current peak (I_p).

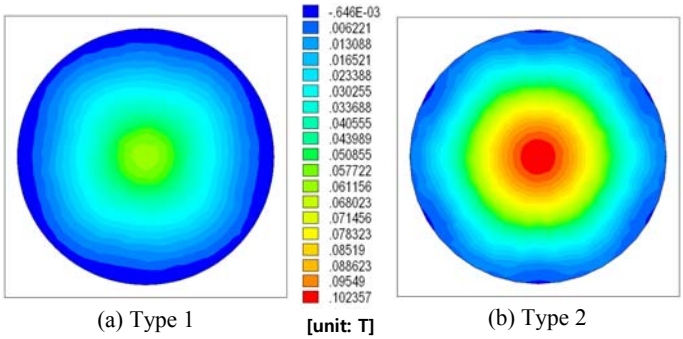

(a) Type 1 (b) Type 2

Figure 5 AMF distributions on the intermediate plane of the gap at current zero (I_o).

analyses. The horizontal axis indicates the radial positions on the contact surface and the vertical axis shows the AMF flux density (B_Z), respectively. Curves are plotted as a function of the phase angle (θ), which varies with a time ($\theta=\omega t$), applied AC is presented as follows:

$$I(t) = 30000\sqrt{2}\cos(\omega t)\ [\mathrm{A}] \quad (6)$$

As shown in Fig. 3, there are two peak currents (I_p=42.4kA at θ=0 and π) and a minimum value of current zero (I_0=0kA at $\theta=\pi/2$). It is shown that AMF values of two series simulations are agreed well with the overall trends each other. Some deviations should be caused by the governing equations concerned in the programs.

Two different types of AMF contacts are calculated as shown in Fig. 1. The AMF flux density (B_Z) on the intermediate plane of the arc gap according to the two different contacts are illustrated in Figs. 4 and 5 at current peak (I_p) and zero (I_0), respectively. As shown in Fig. 4, some peak areas are locally displayed with two different configurations of the contacts. The maximum value of B_Z is approximately 346mT at Type 1 and 372mT at Type 2, respectively. In the case of Type 1, it has four low areas because of its four slots. In the case of Type 2, it has relatively uniform AMF flux density distributions across the entire contact surface within the range of the contour legend. Figure 5 shows the AMF flux density distributions of residual AMF generated by eddy current at current zero. Both have the peak areas at the center, each maximum value is 87mT and

125mT in accordance with Types 1 and 2, and it decreases azimuthally along the radial direction. If a residual AMF is high, it restricts the diffusion of residual plasma after the arc is distinguished, and thus it makes a recovery of insulation strength. Since it also leads to strong erosion at the contact surface, lowering the residual AMF can be a way to improve the performance of the VI with the AMF contact.

According to the experimental results by Schulman [14], there is a critical AMF value that the diffused vacuum arc mode turned to be the constricted arc mode. The critical AMF was defined as follows:

$$B_{crit} \geq 3.9(I_p - a) \text{ [mT]} \quad (7)$$

Here, I_p is a peak current (kA), a is a particular constant which is applied commonly used empirical value (a=9). From the above formula, the critical AMF B_{crit} is about 130mT. And thus, the predicted results named the effective arc area (A_{eff}), where the AMF strength is stronger than the critical value, are depicted in Fig. 6. A_{eff} is about 71.0 percent for Type 1 and 89.8 percent for Type 2. Although Type 1 has a large amount of maximum AMF values, in the case of Type 2, the mean AMF is higher than that of Type 1. And also the AMF distributed more uniformly in Type 2. As the A_{eff} smaller, the vacuum arc should be constricted with the appearance of the anode spots. In general, the anode activity brings about several problems, e.g., deterioration of the contact features by erosion, degradation of the dielectric strength, and thus the ability of interruption etc. Therefore, it is necessary to maximize the A_{eff} to avoid the influence of the anode activities.

The AMF flux distributions on the intermediate plane of the arc gap are depicted in Fig. 7 as a function of the phase angle. It is shown that the curves have almost symmetrical shapes at two current peak levels (I_p=42.4kA at θ=0 and π). One can see a hollow region at the top of the curves. It indicates an effect of the eddy current from the configuration of the current paths. From the AMF flux distributions, it can be seen that, although the current is zero (I_0=0kA at θ=π/2), there exists the residual AMF which is generated by the eddy current. This residual AMF prevents the residual plasma to disperse, and as a result,

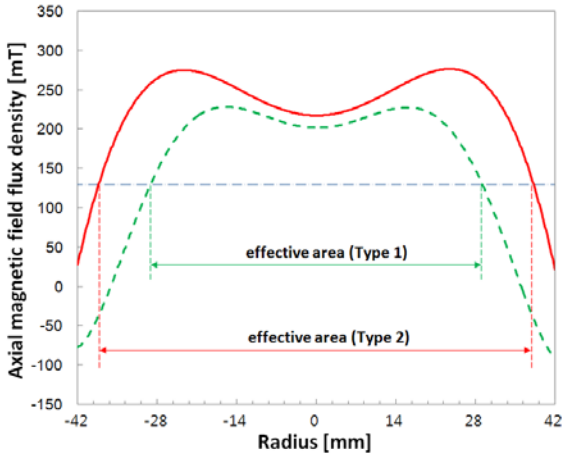

Figure 6 Variation of the effective arc area with AMF distributions on the contact surface.

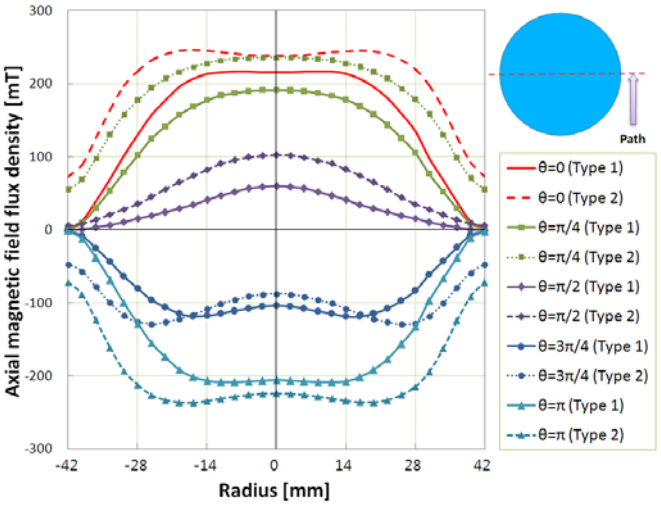

Figure 7 Transient AMF distributions on the intermediate plane of the arc gap.

the dielectric recovery strength is reduced. Since the arc current should be interrupted with the minimum damage to the contact at the current zero instant, it is required to find out the proper contact geometry for the reduction of the residual AMF.

From the relationship between the current and the magnetic field, it is obtained the Joule heat generation from the magnetic analysis. The Joule heat distributions on the contact surface are displayed in Figs. 8 and 9. Since the Joule heat is induced by the current flows, its contours follow the spread of current. Both have the maximum values at the near the slots. In the case of Type 1, a higher range of the Joule heat concentration regions are revealed while Type 2 has relatively uniform distributions throughout the surface.

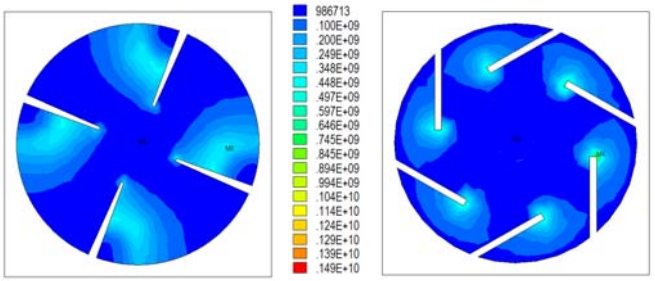

(a) Type 1 (b) Type 2

Figure 8 Joule heat distribution on the anode surface at I_p.

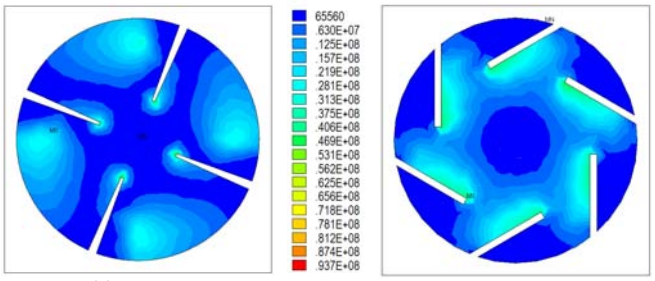

(a) Type 1 (b) Type 2

Figure 9 Joule heat distribution on the anode surface at I_0.

CONCLUSIONS

In this work, three-dimensional electro-magnetic analyses were carried out with two different types of AMF contacts. In order to validate the calculation method, two series of results on the cup-type AMF contacts were compared with a commercial package. AMF flux density values of two series simulations were agreed well with the overall trends each other. From the results of two different types of AMF electrodes, the maximum B_z was locally appeared with the respective number of the slots on the contact surfaces. The residual B_z can be observed at current zero, which is caused by the eddy current effect, it should be reduced because of its harmfulness as a cause of the erosion of the electrode. The effective arc area (A_{eff}) based on the critical AMF value (B_{crit}) was also compared. For the small A_{eff}, the anode spot should be activated which brings about several problems. Consequently, it is required that AMF flux density has not only higher value but also uniform distributions throughout the contact surface. From the relationship between the current and the magnetic field, the Joule heat generation obtained by the electro-magnetic analysis. For the future work, the obtained magnetic analysis data will be coupled with the hydrodynamic governing equations as the input source terms of the MHD multiphysics analysis.

REFERENCES

[1] Schellekens, H., The high-current vacuum arc in an axial magnetic field: An experimental investigation, *J. Phys. D: Appl. Phys*., Vol. 54, pp. 144-149, 1983.

[2] Heberlein, J.V.R. and Gorman, J.G., The high current metal vapour arc column between separating electrodes, *IEEE Trans. Plasma Sci*., Vol. PS-8, pp. 283-288, 1980.

[3] Kimblin, C.W. and Voshall, R.E., Interruption ability of vacuum interrupters subjected to axial magnetic fields, *Proc. IEE*, Vol. 119, pp. 1754-1758, 1972.

[4] Rondeel, W.G.J., The vacuum arc in an axial magnetic field, *J. Phys. D: Appl. phys*., Vol. 8, pp. 934-942, 1975.

[5] Agarwal, M.S. and Holmes, R., Arcing voltage of the metal vapor vacuum arc, *J. Phys. D: Appl. Phys*., Vol. 17, pp. 757-767, 1984.

[6] Nemchinsky, V.A., Vacuum arc in axial magnetic field, in *Proc. XIV ISDEIV*, Santa Fe, NM, pp. 260-262, 1990.

[7] Thomas E. Browne, Circuit Interruption: Theory and Techniques, *Marcel Dekker, Inc*., New York, Chap. 12, pp. 459-472, 1984.

[8] Yanabu, S., Souma, S., Tamagawa, T., Yamashita, S. and Tsutsumi, T., Vacuum arc under an axial magnetic fields and its interruption ability, *Proc. IEE*., Vol. 126, pp. 313-320, 1979.

[9] Bestel, F. and Stoving, P., axial magnetic field interrupters in autorecloser applications, *Proc. 17th ISDEIV*, Berkeley, pp. 1045-1050, 1996.

[10] Schellekens, H., Shang, W. and Lenstra, K., Vacuum interrupter design based on arc magnetic field interaction for horseshoe electrode, *IEEE Trans. Plasma Sci*., Vol. 21, pp. 469-473, 1993.

[11] Fenski, B., Heimbach, M., Lindmayer, M. and Shang, W.K, Characteristics of a vacuum switching contact based on bipolar axial magnetic field, *IEEE Trans. Plasma Sci*., Vol. 27, pp. 949-953, 1999.

[12] Fink, H., Heimbach, M. and Shang, W.K., Vacuum interrupters with axial magnetic field contacts based on bipolar and quadrupolar design, *IEEE Trans. Plasma Sci*., Vol. 29, pp. 738-743, 2001.

[13] Ha, D.Y., Kang, H.B, Choi S.K. and Choi, K.H., A study on the effect of the contact electrode slits in the vacuum interrupter with axial magnetic field type, *J. of KIEEME (in Korean)*, Vol. 15, pp. 822-829, 2002.

[14] Schulman, M.B., Slade, P.G. and Heberlein, J.V.R., Effect of an axial magnetic field upon the development of the vacuum arc between opening electric contacts, *IEEE Trans. CHMT*, Vol. 16, pp. 180-189, 1993.